Progress In Electromagnetics Research, Vol. 126, 521–538, 2012

INVESTIGATION OF EFFECTIVE PLASMA FREQUENCIES IN ONE-DIMENSIONAL PLASMA PHOTONIC CRYSTALS

C.-J. Wu[1,*], T.-J. Yang[2], C.-C. Li[1], and P.-Y. Wu[1]

[1]Institute of Electro-Optical Science and Technology, National Taiwan Normal University, Taipei 116, Taiwan, R.O.C.

[2]Department of Electrical Engineering, Chung Hua University, Hsinchu 300, Taiwan, R.O.C.

Abstract—In this work, a detailed investigation on the effective plasma frequency $f_{p,\,eff}$ for one-dimensional binary and ternary plasma-dielectric photonic crystals is made. We extract and then analyze the effective plasma frequency from the calculated photonic band structures at distinct conditions. In the binary photonic crystal, it is found that $f_{p,\,eff}$ in a photonic crystal is usually smaller than the plasma frequency f_p of a bulk plasma system. $f_{p,\,eff}$ will increase when the electron concentration in the plasma layer increases. It also increases as the thickness of the plasma layer increases, but decreases with the increase in the thickness of dielectric layer. In the ternary photonic crystal, $f_{p,\,eff}$ is shown to be decreased compared to that of in the binary one. Our results are compared with the analytical expression for $f_{p,\,eff}$ derived from the concept of effective medium. Fairly good consistence has been obtained for both results. Additionally, a discussion on the effect of loss on $f_{p,\,eff}$ is also given. The study is limited to the case of normal incidence.

1. INTRODUCTION

Over the past two decades, photonic crystals (PCs) have attracted much attention since the pioneering works of Yablonovitch [1] and John [2]. PCs are artificially periodic multilayer structures and possess photonic band gaps (PBGs) which are formed due to the Bragg scattering in the periodic structure. PBGs are physically analogous to the electronic band gaps (EBGs) in semiconducting materials or solids.

Received 5 March 2012, Accepted 27 March 2012, Scheduled 4 April 2012

* Corresponding author: Chien-Jang Wu (jasperwu@ntnu.edu.tw).

PCs are commonly referred to as the PBG materials. Engineering the PBGs for realizing some useful photonic and optoelectronic devices continues to be of much interest to the community.

For a PC made of all dielectric constituents is called a dielectric-dielectric photonic crystal (DDPC). A simple one-dimensional DDPC is known to have an omnidirectional PBG [3, 4]. Depending on the constituent materials, PCs have many other types in addition to the DDPCs. For instance, if one of the constituents is replaced by a metal, then we have a metal-dielectric photonic crystal (MDPC). The MDPCs can be used to enhance the wave transmission in the visible region [5, 6]. In addition, with the inherent metallic loss, the photonic band structure in an MDPC is complex [7, 8]. Meanwhile, photonic crystals containing superconducting materials also attract much attention and they are referred to as superconductor-dielectric photonic crystals (SDPCs) [9–12]. The use of superconductor in an SDPC makes it tunable because the permittivity of a superconductor is strongly dependent on the temperature and the magnetic field as well [13]. Both metal and superconductor have a common feature of dispersion, namely their permittivities are dependent on the frequency.

Another type of photonic crystals called the plasma photonic crystal (PPC) was first proposed by Hojo and Mase in 2004 [14]. Since then, there have been many reports on the PPCs [15–17]. In a bulk plasma system, the relative permittivity takes the form

$$\varepsilon(\omega) = 1 - \frac{\omega_p^2}{\omega^2 - j\gamma\omega}, \tag{1}$$

where γ, the loss factor, is the plasma collision frequency and the plasma frequency ω_p, which is dependent on the electron density, and written as

$$\omega_p = 2\pi f_p = \left(\frac{Ne^2}{m\varepsilon_0}\right)^{1/2}, \tag{2}$$

where N is the electron concentration, m the mass of free electron, e the electronic charge, and ε_0 the permittivity of vacuum. It is clear that changing N will cause the plasma frequency to be changed, which, in turn, leads to a variation in the permittivity of a plasma system. With a variable permittivity, a plasma system can be regarded as a dispersive medium. In the first order approximation where loss is negligible, the wave propagation in a plasma system can be simply characterized by f_p. For frequency higher than f_p, the plasma is transparent to the incident wave since the permittivity (or refractive index) is positive. On the other hand, wave propagation in a plasma system is forbidden when the frequency is lower than f_p. Thus, the plasma frequency, f_p can be defined as a cutoff (or characteristic)

frequency for a bulk plasma system. It should be mentioned that the expression of permittivity in Eq. (1) is based on the use of convention $\exp(j\omega t)$ for the time part, as also will be taken in the following Eq. (3).

However, electromagnetic waves can, indeed, propagate in a PPC even at the frequencies less than f_p due to the structural periodicity. The lowest frequency, at which wave propagation can start to happen, is defined as an effective plasma frequency $f_{p,\,eff}$ for a PPC system. The concept of effective plasma frequency enables us to replace the PPC by a semi-infinite effective plasma medium which is characterized by an effective permittivity together with $f_{p,\,eff}$ [18]. It will be later shown that $f_{p,\,eff}$ is always smaller than f_p. The frequency range of 0–$f_{p,\,eff}$ is thus called the low-frequency gap. Obviously, the existence of this low-frequency gap in the PPC is fundamentally different from the DDPC, which has no such low-frequency gap.

The purpose of this paper is to give a more detailed analysis on the effective plasma frequency for both the binary and ternary PPCs. The binary PCs are most common structures in the literature reports and experimental studies are now available [19–23]. However, ternary PCs have also attracted much attention recently [24–30]. Naumov and Zheltikov first showed that multicomponent (ternary) one-dimensional (1D) PBG structures provide additional degree of freedom in dispersion control compared to binary 1D PBG structure [31]. Motivated by these facts, in this work, effective plasma frequencies for these two structures will be considered. In the binary PPC, we would like to investigate how the effective plasma frequency can be influenced by the thicknesses of plasma and dielectric layers as well as the electron concentration of the plasma layer. In the ternary PPC, the plasma layer is sandwiched by two dielectrics with different permittivities in each period. The role played by the additional dielectric layer in the effective plasma frequency will be analyzed and illustrated.

The paper is organized as follows. Section 1 is the introductory part. The theoretical formulations are described in Section 2. In Section 3, we present and discuss the numerical results. We conclude a summary in Section 4.

2. BASIC EQUATIONS

Let us first consider the binary PPC shown in the upper panel of Figure 1, in which the constituent dielectric layer A has a permittivity of ε_A, and the constituent layer B is a plasma with a permittivity of ε_B (as given in Eq. (1)). The refractive indices of A and B are given by $n_p = \sqrt{\varepsilon_p}$, $p = A$ and B, respectively. The spatial periodicity is defined by $a = d_A + d_B$. The refractive index profile can be expressed

as

$$n(x) = \begin{cases} n_A, & ma < x < ma + d_A, \\ n_B, & ma + d_A < x < (m+1)\,a, \end{cases} \quad m = 0, \pm 1, \pm 2, \ldots \ . \tag{3}$$

For the transverse electric (TE) wave, the electric field propagating in the x-direction and positive z-direction can be written as $\mathbf{E}(x, z, t) = \hat{y}E(x)\, e^{j(\omega t - \beta z)}$, where β is the (constant) tangential component of the wave vector of modulus $k_0 n(x)$ inside the medium and the function $E(x)$ satisfies the Helmholtz equation,

$$\frac{d^2}{dx^2} E(x) + \left[k_0^2 n^2(x) - \beta^2\right] E(x) = 0, \tag{4}$$

inside the system layers, where $k_0 = \omega/c$ is the vacuum wave number. Eq. (4), in fact, is a form of Hill's equation [32]. Solutions for Eq. (4) can be written as a linear combination of forward and backward waves, namely

$$E(x) = \begin{cases} a_n e^{-jk_{A,x}x} + b_n e^{jk_{A,x}x}, & 0 < x < d_A \\ c_n e^{-jk_{B,x}x} + d_n e^{jk_{B,x}x}, & d_A < x < a, \end{cases} \ . \tag{5}$$

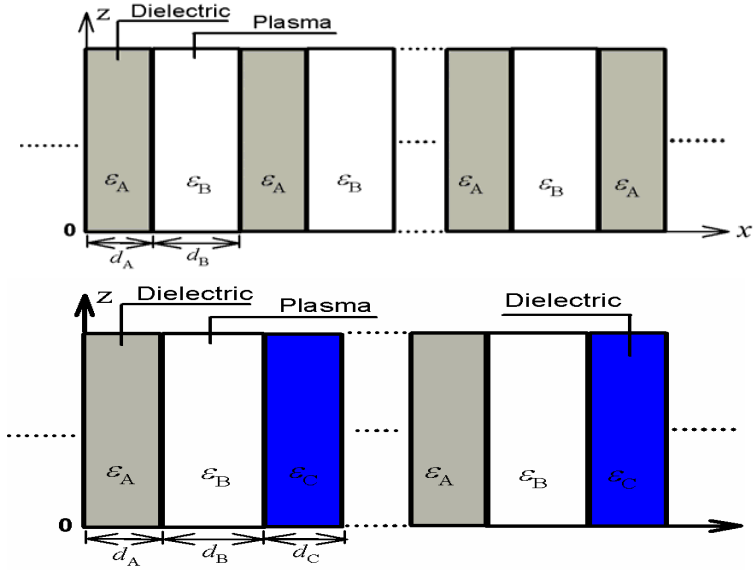

Figure 1. The structures of the infinite binary (upper panel) and ternary (lower panel) plasma-dielectric photonic crystals, where layer A and C are dielectrics and the plasma occupies layer B. The corresponding thicknesses and permittivities are denoted by d_A, d_B, d_C, and ε_A, ε_B, ε_C, respectively.

where a_n, b_n, c_n, and d_n are unknown constants, and the normal component of wave number is given by

$$k_{A,x} = \sqrt{k_0^2 n_A^2 - \beta^2} = k_0 n_A \cos\theta_A, \tag{6}$$

$$k_{B,x} = \sqrt{k_0^2 n_B^2 - \beta^2} = k_0 n_B \cos\theta_B, \tag{7}$$

where θ_A and θ_B are the ray angles in layers A and B, respectively, which are related by the Snell's law of refraction. By capitalizing on the continuous boundary conditions at $x = 0$, d_A, and $d_A + d_B$, it is direct to construct the following matrix relationship,

$$\begin{pmatrix} a_{n-1} \\ b_{n-1} \end{pmatrix} = \begin{pmatrix} A & B \\ C & D \end{pmatrix} \begin{pmatrix} a_n \\ b_n \end{pmatrix}, \tag{8}$$

where A, B, C, and D are the matrix elements of the single period translational matrix that relates the amplitudes of forward and backward waves a_{n-1} and b_{n-1} in one layer of a period to those of the equivalent layer in the next period. Expressions for the matrix elements A, B, C, and D are written by [33]

$$A = e^{jk_{A,x}d_A}\left[\cos\left(k_{B,x}d_B\right) + \frac{j}{2}\left(\frac{k_{B,x}}{k_{A,x}} + \frac{k_{A,x}}{k_{B,x}}\right)\sin\left(k_{B,x}d_B\right)\right], \tag{9}$$

$$B = e^{-jk_{A,x}d_A}\left[\frac{1}{2}j\left(\frac{k_{B,x}}{k_{A,x}} - \frac{k_{A,x}}{k_{B,x}}\right)\sin\left(k_{B,x}d_B\right)\right], \tag{10}$$

$$C = e^{jk_{A,x}d_A}\left[-\frac{1}{2}j\left(\frac{k_{B,x}}{k_{A,x}} - \frac{k_{A,x}}{k_{B,x}}\right)\sin\left(k_{B,x}d_B\right)\right], \tag{11}$$

$$D = e^{-jk_{A,x}d_A}\left[\cos\left(k_{B,x}d_B\right) - \frac{1}{2}j\left(\frac{k_{B,x}}{k_{A,x}} + \frac{k_{A,x}}{k_{B,x}}\right)\sin\left(k_{B,x}d_B\right)\right], \tag{12}$$

In addition, for a periodic structure, according to the Floquet-Bloch theorem, the electric-field solution must be cast as a Bloch form, namely

$$E_K(x,t) = E_K(x)\, e^{-jKx} e^{j\omega t}, \tag{13}$$

where the amplitude is a periodic function of a, i.e., $E_K(x + ma) = E_K(x)$. The Bloch wave vector K can be determined by the half trace of the translational matrix in Eq. (8), i.e.,

$$\cos(Ka) = \frac{1}{2}(A + D). \tag{14}$$

The explicit expression of Eq. (14) is given by

$$\cos(Ka) = \cos\left(k_{A,x}d_A\right)\cos\left(k_{B,x}d_B\right) - \frac{1}{2}\left(\frac{k_{A,x}}{k_{B,x}} + \frac{k_{B,x}}{k_{A,x}}\right)\sin\left(k_{A,x}d_A\right)\sin\left(k_{B,x}d_B\right). \tag{15}$$

For the transverse magnetic (TM) wave, the above-mentioned electric field should be replaced by the magnetic field, and then the expression in Eq. (15) can be written by

$$\begin{aligned}\cos(Ka) &= \cos(k_{A,x}d_A)\cos(k_{B,x}d_B) \\ &\quad -\frac{1}{2}\left(\frac{n_B^2 k_{A,x}}{n_A^2 k_{B,x}}+\frac{n_A^2 k_{B,x}}{n_B^2 k_{A,x}}\right)\sin(k_{A,x}d_A)\sin(k_{B,x}d_B)\,, \quad (16)\end{aligned}$$

In general, the Bloch wave number K appearing in the left hand side of Eq. (15) or (16) is complex-valued, i.e., $K = K_r - jK_i$. For frequencies at which K's are purely real, we have the pass band. On the other hand, we will have a PBG if the imaginary part K_i exists in the solution for K.

For the ternary plasma PC shown in the lower panel of Figure 1, each period is now made of three layers, i.e., $A/B/C$, where another dielectric layer C is added. The spatial periodicity is denoted by $a = d_A + d_B + d_C$. The field solution is also given in Eq. (13) and, in this case, the Bloch wave number can be computed by the following equation,

$$\begin{aligned}\cos(K\Lambda) &= \cos(k_{A,x}d_A)\cos(k_{B,x}d_B)\cos(k_{C,x}d_C) \\ &\quad -\frac{1}{2}\left(\frac{n_A}{n_B}+\frac{n_B}{n_A}\right)\sin(k_{A,x}d_A)\sin(k_{B,x}d_B)\cos(k_{C,x}d_C) \\ &\quad -\frac{1}{2}\left(\frac{n_B}{n_C}+\frac{n_C}{n_B}\right)\cos(k_{A,x}d_A)\sin(k_{B,x}d_B)\sin(k_{C,x}d_C) \\ &\quad -\frac{1}{2}\left(\frac{n_A}{n_C}+\frac{n_C}{n_A}\right)\sin(k_{A,x}d_A)\cos(k_{B,x}d_B)\sin(k_{C,x}d_C)\,. \quad (17)\end{aligned}$$

It should be noted that Eq. (17) holds only for the normal incidence, i.e., the ray angle is $\theta_i = 0$. In this study, for both the binary and ternary PPCs, we shall limit to the case of normal incidence to investigate the effective plasma frequency.

3. NUMERICAL RESULTS AND DISCUSSION

3.1. Effective Plasma Frequency in a Binary PPC

Let us now present the numerical analysis on the effective plasma frequency for the binary PPC. In the following calculations, we shall consider the normal incidence and lossless case in plasma, i.e., $\gamma = 0$. The calculated photonic band structure (PBS) is plotted in Figure 2, in which we take thicknesses $d_A = 0.5\,\text{mm}$, $d_B = 5\,\text{mm}$, and the dielectric is taken to be a quartz with $n_A = 2$ [15]. In addition, the electron concentration $N = 10^{17}\,\text{m}^{-3}$ is taken. At this concentration,

the calculated bulk plasma frequency is $f_p = 2.84\,\text{GHz}$ according to Eq. (2). As indicated in Figure 2, the starting frequency of the first pass band is defined as the effective plasma frequency $f_{p,\,eff}$ for the binary PPC. The calculated value of $f_{p,\,eff}$ is 2.38 GHz which is smaller than f_p. It can be expected that if $N \to 0$, then $f_{p,\,eff} \to 0$ because $f_p \to 0$, which, in turn, reduces to the case of a simple all-dielectric PC that is known to have the pass band starting from zero-frequency. The lowest band gap at frequency range of 0–$f_{p,\,eff}$ is referred to as the low-frequency gap. The second gap is the common Bragg gap because the permittivity (index of refraction) of plasma is positive there. In this gap, the plasma behaves like a dispersive dielectric material with

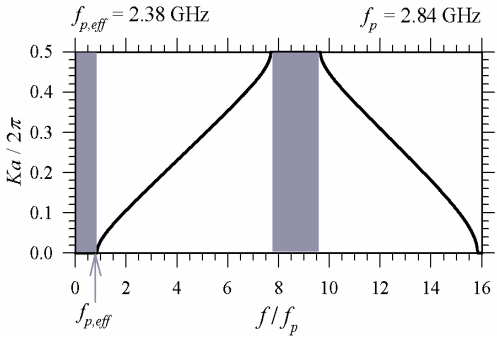

Figure 2. The calculated photonic band structure for a binary PPC with $d_A = 0.5\,\text{mm}$, $d_B = 5\,\text{mm}$ and electron concentration $N = 10^{17}\,\text{m}^{-3}$. The calculated $f_{p,\,eff} = 2.38\,\text{GHz}$ (indicated by arrow) is less than the bulk plasma frequency of $f_p = 2.84\,\text{GHz}$. The shaded areas represent the band gaps.

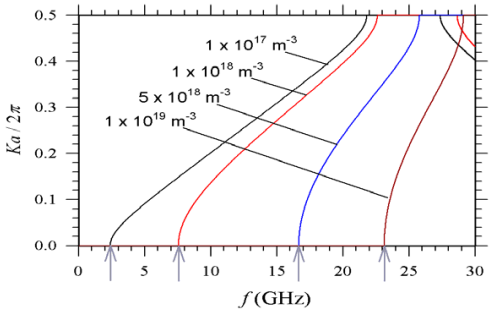

Figure 3. The calculated PBSs at different electron concentrations of $N = 10^{17}$, 10^{18}, 5×10^{18}, and $10^{19}\,\text{m}^{-3}$, respectively. The effective plasma frequency is blue-shifted as N increases.

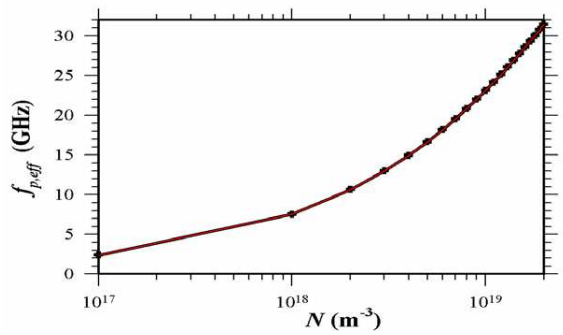

Figure 4. The calculated $f_{p,\,eff}$ versus electron concentration N for a binary PPC with $d_A = 0.5\,\text{mm}$, $d_B = 5\,\text{mm}$.

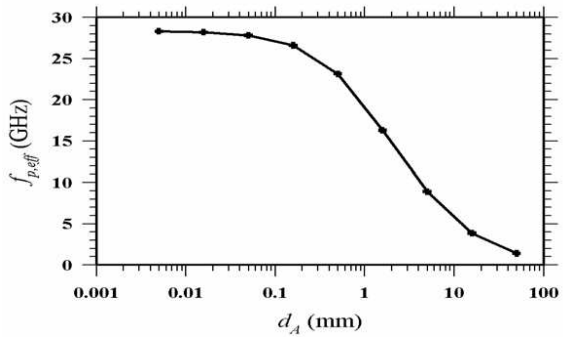

Figure 5. The calculated $f_{p,\,eff}$ versus the thickness of dielectric layer d_A at a fixed carrier concentration $N = 10^{19}\,\text{m}^{-3}$ and $d_B = 5\,\text{mm}$.

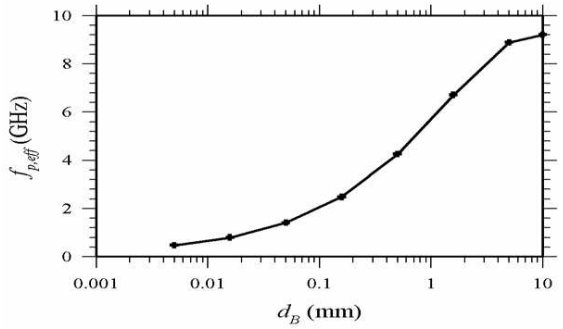

Figure 6. The calculated $f_{p,\,eff}$ versus the thickness of plasma layer d_B at a fixed carrier concentration $N = 10^{19}\,\text{m}^{-3}$ and $d_A = 5\,\text{mm}$.

a real and positive refractive index. The gap edges are $f/f_p = 7.75$ and 9.65, leading to a gap size of $\Delta f = 1.90 f_p$.

Next, with both thicknesses d_A and d_B fixed, the first bands at distinct values of N are plotted in Figure 3, in which it is seen that $f_{p,\,eff}$ (marked by an arrow) will increase as N increases. A plot of $f_{p,\,eff}$ versus N is depicted in Figure 4, in which the values of $f_{p,\,eff}$ are 2.38, 7.54, 16.65, and 23.06 GHz for $N = 10^{17}$, 10^{18}, 5×10^{18}, and $10^{19}\,\mathrm{m}^{-3}$, respectively. The shift in $f_{p,\,eff}$ can be ascribed to the increase in f_p when N is increased. The results shown here are consistent with the experimental data reported in [19]. In Figure 7 of [19], it is seen that the dependence of effective plasma frequency on the electron density has a similar tendency as in Figure 4.

We now investigate how the thickness of the dielectric layer affects the effective plasma frequency. In Figure 5, we plot $f_{p,\,eff}$ as a function of d_A at a fixed value of $N = 10^{19}\,\mathrm{m}^{-3}$ and $d_B = 5\,\mathrm{mm}$. With this concentration, the plasma frequency is calculated to be $f_p = 28.38\,\mathrm{GHz}$. At $d_A = 0.05$ and 5 mm, we have $f_{p,\,eff} = 27.81$ and 8.89 GHz, respectively. It can be seen that, for d_A larger than 0.1 mm, the decrease in $f_{p,\,eff}$ is salient. However, for a thinner dielectric layer like $d_A < 0.1\,\mathrm{mm}$, the effective plasma frequency, $f_{p,\,eff}$ of PPC is approaching to the bulk plasma frequency, f_p. It indicates that the effect of structural periodicity can be pronounced when the thickness of dielectric layer must be preferably larger than 0.1 mm if plasma layer is at 5 mm. Based on the result in Figure 5, it is expected that the effective plasma frequency will be an increasing function of the thickness of plasma layer. Indeed, it can be seen in Figure 6, where $f_{p,\,eff}$ versus d_B is plotted at the conditions of $N = 10^{19}\,\mathrm{m}^{-3}$ and $d_A = 5\,\mathrm{mm}$. It is seen that $f_{p,\,eff}$ is blue-shifted when d_B is increased. At $d_B = 0.5\,\mathrm{mm}$, $f_{p,\,eff} = 4.26\,\mathrm{GHz}$, and $f_{p,\,eff} = 1.41\,\mathrm{GHz}$ for $d_B = 0.05\,\mathrm{mm}$.

The above dependences of effective plasma frequency are extracted by the calculated PBSs. We now compare them with the analytical expression for the effective plasma frequency in a PC. Here, we briefly review the derivation of effective plasma frequency made by Manzanares-Martinez [18]. Since the permittivity is a periodic function, it can be expanded as a Fourier series, namely

$$\varepsilon(x,\omega) = \sum_{G_N} \tilde{\varepsilon}(G_N) e^{jG_N x} = \tilde{\varepsilon}(0) + \sum_{G_N \neq 0} \tilde{\varepsilon}(G_N) e^{jG_N x}, \qquad (18)$$

where $G_N = 2\pi N/a$ is the reciprocal lattice vector, and N is an integer.

The Fourier coefficients at $N = 0$ and $N \neq 0$ are respectively given by

$$\tilde{\varepsilon}(0) = \phi\varepsilon_B + (1-\phi)\,\varepsilon_A, \tag{19}$$

$$\tilde{\varepsilon}(G_N) = \frac{\varepsilon_A - \varepsilon_B}{jG_N a}\left(1 - e^{-jG_N d_A}\right), \tag{20}$$

where $\phi = d_B/a$ is the filling factor of the plasma layer in one unit cell. The effective permittivity can be taken as the average value in one period, namely

$$\varepsilon_{\mathit{eff}}(\omega) = \langle \varepsilon(x,\omega)\rangle = \frac{1}{a}\int_0^a dx'\,\varepsilon\left(x - x', \omega\right). \tag{21}$$

Substituting the Fourier series, Eqs. (18)–(20), together with the permittivity in Eq. (1) leads to the effective permittivity of the effective bulk plasma which can effectively replace a structure of PPC, namely

$$\varepsilon_{\mathit{eff}}(\omega) = \varepsilon_{0,\,\mathit{eff}} - \frac{\phi\omega_p^2}{\omega^2 - j\gamma\omega}, \tag{22}$$

where $\varepsilon_{0,\,\mathit{eff}} = \varepsilon_A + \phi(1-\varepsilon_A)$ is the effective static permittivity. According to Eq. (22), it is natural to define the effective plasma frequency as

$$\omega_{p,\,\mathit{eff}} = 2\pi f_{p,\,\mathit{eff}} = \phi^{1/2}\omega_p\,. \tag{23}$$

However, this is not what we want because the first term in the right hand side of Eq. (22) is not one, as expressed in Eq. (1). In fact, the effective plasma frequency is best extracted by considering the lossless case ($\gamma = 0$). In this case, the effective plasma frequency is redefined as a characteristic frequency at which $\varepsilon_{\mathit{eff}}(\omega) = 0$. Based on Eq. (22) an analytical expression for the effective plasma frequency can thus be derived as follows,

$$f_{p,\,\mathit{eff}} = \frac{\phi^{1/2}\omega_p}{2\pi\sqrt{\varepsilon_A + \phi(1-\varepsilon_A)}}\,. \tag{24}$$

Eq. (24) is the main expression that describes the effective plasma frequency for a binary photonic crystal system. It can be seen that $f_{p,\,\mathit{eff}}$ relies on the filling factor and the plasma frequency of plasma layer, and the permittivity of dielectric layer. Taking the conditions in Figure 2, Eq. (24) gives $f_{p,\,\mathit{eff}} = 2.398\,\mathrm{GHz}$, which shows a good agreement with the result in Figure 2. Again, in Figure 5, with $d_A = 0.05$, $d_B = 5\,\mathrm{mm}$, and $N = 10^{19}\,\mathrm{m}^{-3}$, Eq. (24) yields $f_{p,\,\mathit{eff}} = 27.82\,\mathrm{GHz}$, nicely consistent with that shown in Figure 5.

3.2. Effective Plasma Frequency in a Ternary PPC

Let us now investigate the effective plasma frequency in a ternary PPC shown in the lower panel of Figure 1. Here, the additional layer C is taken to be MgF_2 whose refractive index is $n_C = 1.38$ [30]. With the same material parameters for layers A and B in the calculation of Figure 2 and the thickness of MgF_2 being $d_C = 0.5\,\text{mm}$, the calculated PBS is pictured in Figure 7. Again, $f_{p,\,eff}$ is smaller than f_p. It can be further seen that the PBS is red-shifted compared to that of the binary PPC in Figure 2. The shift causes the effective plasma frequency to be smaller than that of the binary PPC. The calculated value is $f_{p,\,eff} = 2.24\,\text{GHz}$, as indicated by the vertical arrow. In addition, the second gap (with a center frequency around $8f_p$) is also enhanced when compared to the binary one in Figure 2 because the gap edges are $f/f_p = 6.85$ and 8.80, and hence the gap size is $\Delta f = 1.95 f_p$.

Next, we vary the thickness of layer C and see what will happen in the effective plasma frequency. The calculated $f_{p,\,eff}$ is shown in Figure 8. It can be seen from the figure that $f_{p,\,eff}$ will be moved to the lower frequency as the thickness d_C increases. The values of $f_{p,\,eff}$ at $d_C = 0.1$, 0.5, 1, 5 and 10 mm are $0.83f_p$, $0.79f_p$, $0.75f_p$, $0.55f_p$, and $0.44f_p$, respectively. The addition of dielectric layer C in the ternary PPC will decrease the effective plasma frequency compared to the binary PPC. For d_C less than 1 mm, the shift in $f_{p,\,eff}$ is not so substantial as that for greater than 1 mm.

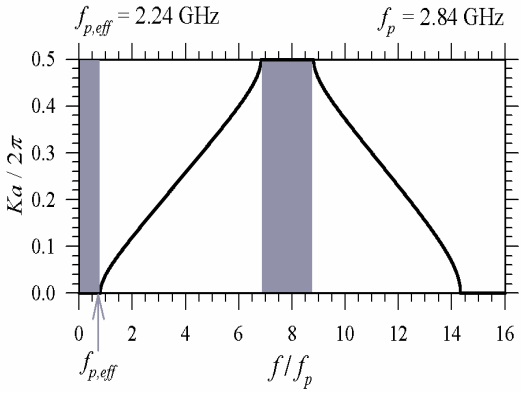

Figure 7. The calculated photonic band structure for a ternary PPC with $d_A = 0.5\,\text{mm}$, $d_B = 5\,\text{mm}$, $d_C = 0.5\,\text{mm}$ and electron concentration $N = 10^{17}\,\text{m}^{-3}$. The calculated $f_{p,\,eff} = 2.24\,\text{GHz}$ (indicated by arrow) is less than the effective plasma frequency ($f_{p,\,eff} = 2.38\,\text{GHz}$) of a binary PPC and the bulk plasma frequency ($f_p = 2.84\,\text{GHz}$). The shaded areas represent the band gaps.

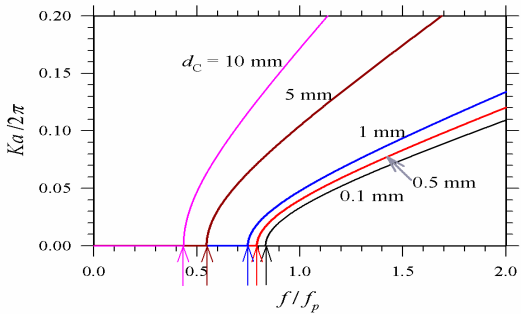

Figure 8. The calculated effective plasma frequency (marked by the vertical arrow) for a ternary PPC with $d_A = 0.5\,\text{mm}$, $d_B = 5\,\text{mm}$, and electron concentration $N = 10^{17}\,\text{m}^{-3}$ for different thicknesses $d_C = 0.1$, 0.5, 1, 5, and 10 mm, respectively.

In order to quantitatively explain the blue-shift in $f_{p,\,eff}$ in the ternary PPC, we can repeat the derivations from Eqs. (18)–(24) and then arrive at the following similar expressions, i.e., Eq. (19) is revised as

$$\tilde{\varepsilon}\,(0) = \phi\,\varepsilon_B + (1-\phi)\,\varepsilon_{av}. \tag{25}$$

Most importantly, Eq. (24) for the effective plasma frequency is now given by

$$f_{p,\,eff} = \frac{\phi^{1/2}\omega_p}{2\pi\sqrt{\varepsilon_{av} + \phi\,(1-\varepsilon_{av})}}, \tag{26}$$

where

$$\varepsilon_{av} = \frac{\varepsilon_A d_A + \varepsilon_C d_C}{d_A + d_C}, \tag{27}$$

is the average permittivity of two dielectric layers A and C. This enables us to treat the ternary PPC as an effective binary PPC by combining layers A and C as an equivalent layer with a permittivity of ε_{av}. As a test of Eq. (26), we take $d_A = 0.5\,\text{mm}$, $d_C = 0.5\,\text{mm}$, $n_A = 2(\varepsilon_A = 2^2)$, and $n_C = 1.38(\varepsilon_C = 1.38^2)$, we have $\varepsilon_{av} = 2.9522$. In this case, with $d_B = 5\,\text{mm}$, the filling factor of the plasma layer is $\phi = d_B/a = 5/6$. Then, using Eq. (26), we arrive at $f_{p,\,eff} = 0.7929 f_p$, which is in good agreement with that in Figure 8. Similarly, if thickness of layer C is decreased to $d_C = 0.1\,\text{mm}$, then $\phi = d_B/a = 5/5.6$, and $\varepsilon_{av} = 3.6507$. In this case, Eq. (26) leas to $f_{p,\,eff} = 0.8339 f_p$, which again agrees well with Figure 8. Thus, we have successfully explained the red-shift in $f_{p,\,eff}$ when the thickness of layer C is increased. The analytical expression in Eq. (26) gives a good agreement with the numerical results.

3.3. Effective Plasma Frequency in the Presence of Loss

In the above discussion, we have consider the lossless case, i.e., $\gamma = 0$ in Eq. (1). The effective plasma frequency can be well explained by the analytical expressions such as Eqs. (24) and (26). However, in the presence of loss it is not possible to derive a simple analytical expression for the effective plasma frequency because the effective permittivity in Eq. (22) is a complex function. In addition, the photonic band structure becomes complex, that is, the Bloch wave number K together with $\cos(Ka)$ will be complex-valued everywhere, including the PBG as well as the transmission band) [34]. For example, taking the same calculation conditions as in Figure 2 and taking into account the loss of $\gamma = 0.1\omega_p$, the calculated complex photonic band structure is shown in Figure 9. Here, the upper and lower panels are the real and imaginary parts of Bloch wavenumber, respectively. It can be seen that, due to the inclusion of loss, a salient effect on the first band gap is seen. The first PBG in the real part of Bloch wavenumber in Figure 2 is no longer flat, as circled in the upper panel. This non-flat PBG is reflected on the appearance of imaginary part, K_i, as illustrated in the lower panel. These non-flat features in both K_r and K_i are not easy for us to define the effective plasma frequency when the loss is incorporated.

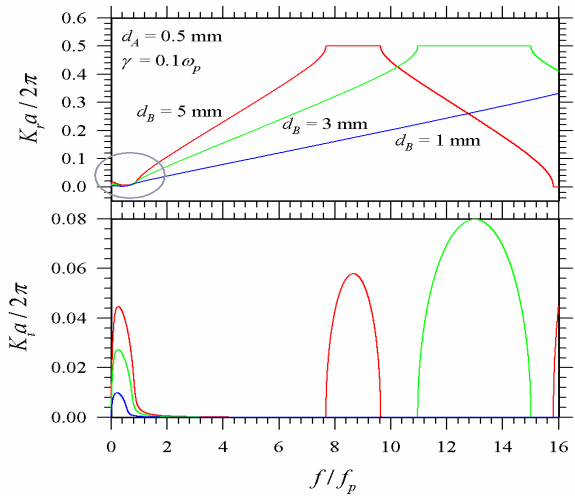

Figure 9. The calculated real (upper panel) and imaginary (lower panel) parts of the Bloch wavenumber at $\gamma = 0.1\omega_p$ for three different thicknesses of plasma layer, $d_B = 5$, 3, and 1 mm, respectively. Here, $d_A = 0.5$ mm, and electron concentration $N = 10^{17}\,\mathrm{m}^{-3}$.

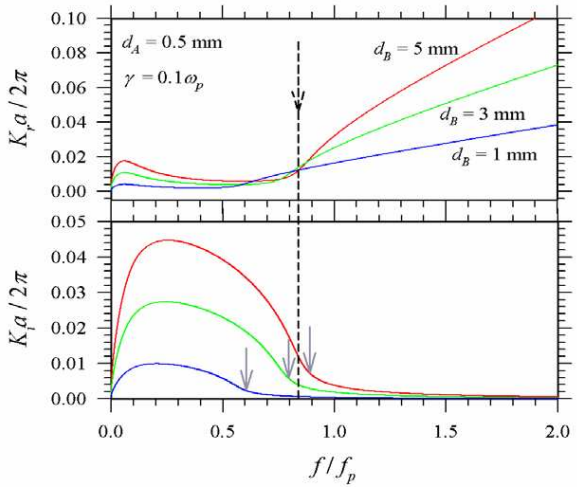

Figure 10. The calculated real (upper panel) and imaginary (lower panel) parts of the Bloch wavenumber for the first PBG of Figure 9.

In order to define the effective plasma frequency of a PPC in the presence of loss, we take a close look at the first PBG of Figure 9, as shown in Figure 10. Here, the vertical dashed arrow-line marks the effective plasma frequency for $d_B = 5\,\text{mm}$ in the absence of the loss, as depicted in Figure 2. From Figure 10, we see that both K_r and K_i first concave downwards and then upwards. For convenience, we define the effective plasma frequency as the turning position at which K_i makes a change from concave down to concave up. We indicate them with gray arrows. The effective plasma frequency at $d_B = 5\,\text{mm}$ with loss is somewhat larger than that of without loss (the vertical dashed line). The effective plasma frequency is the shifted to the lower frequency as the thickness of plasma layer decreases, which is like in the absence of the loss in Figure 6. In addition, it is worth mentioning that the presence of loss in PPC leads to a so-called complex photonic band structure. Thus, the criterion of the definition of effective plasma frequency is not unique [18, 35]. Finally, it is worth mentioning that the experimental verification of the complex photonic band structure in a lossy PPC has been available [36].

4. CONCLUSION

In summary, we have investigated the effective plasma frequency for the binary and ternary plasma photonic crystals in the case of normal

incidence. We find that, for both the binary and ternary PPCs, the effective plasma frequency is always smaller than the bulk plasma frequency of the plasma system. In a binary PPC, the effective plasma frequency is increased as the electron concentration increases. It is also increased as the thickness of the plasma layer increases. However, it will decrease when the thickness of the dielectric layer is increased. In the ternary PPC, it is found that the additional dielectric layer will cause the effective plasma frequency to become smaller compared to the binary one. The calculated results are compared with the analytical expression derived from the effective medium concept. The validity of analytical expression for the effective plasma frequency in a PPC has been verified by the calculated photonic band structure. Good agreement between the results of analytical expression and PBS has been obtained. Finally, we have discussed the definition of effective plasma frequency in the presence of loss. With the loss, the complex photonic band structures enable us to graphically define the effective plasma frequency. However, no analytical expression for the effective plasma frequency can be derived.

ACKNOWLEDGMENT

C.-J. Wu acknowledges the financial support from the National Science Council (NSC) of the Republic of China (R.O.C., Taiwan) under Contract No. NSC-100-2112-M-003-005-MY3 and from the National Taiwan Normal University under NTNU100-D-01.

REFERENCES

1. Yablonovitch, E., "Inhibited spontaneous emission in solid state physics and electronics," *Phys. Rev. Lett.*, Vol. 58, 2059–2062, 1987.
2. John, S., "Strong localization of photons in certain disordered lattices," *Phys. Rev. Lett.*, Vol. 58, 2486–2489, 1987.
3. Fink, Y., J. N. Winn, S. Fan, C. Chen, J. Michel, J. D. Joannopoulos, and L. E. Thomas, "A dielectric omnidirectional reflector," *Science*, Vol. 282, 1679–1682, 1998.
4. Winn. J. N., Y. Fink, S. Fan, and J. D. Joannopoulos, "Omnidirectional reflection from a one-dimensional photonic crystal," *Optics Lett.*, Vol. 23, 1573–1575, 1998.
5. Bloemera, M. J. and M. Scalora, "Transmissive properties of Ag/MgF_2 photonic band gaps," *Appl. Phys. Lett.*, Vol. 72, 1676–1678, 1998.

6. Choi, Y.-K., Y.-K. Ha, J.-E. Kim, H. Y. Park, and K. Kim, "Antireflection film in one-dimensional metallo-dielectric photonic crystals," *Optics Commun.*, Vol. 230, 239–243, 2004.
7. Perze-Rodriguez, F., F. Diaz-Monge, N. M. Makarov, R. Marquez-Islas, and B. Flores-Desirena, "Spatial-dispersion effects in one-dimensional photonic crystals with metallic inclusion," *MSWW 07 Symposium Proceedings*, 92–97, 2007.
8. Soto-Puebla, D., M. Xiao, and F. Ramos-Mendieta, "Optical properties of a dielectric-metallic superlattice: The complex photonic bands," *Phys. Lett. A*, Vol. 326, 273–280, 2004.
9. Bermann, O. L., Y. E. Lozovik, S. L. Eiderman, and R. D. Coalson, "Superconducting photonic crystals," *Phys. Rev. B*, Vol. 74, 092505, 2006.
10. Takeda, H. and K. Yoshino, "Tunable photonic band schemes in two-dimensional photonic crystals composed of copper oxide high-temperature superconductors," *Phys. Rev. B*, Vol. 67, 245109, 2005.
11. Wu, C.-J., M.-S. Chen, and T.-J. Yang, "Photonic band structure for a superconducting-dielectric superlattice," *Physica C*, Vol. 432, 133–139, 2005.
12. Lin, W.-H., C.-J. Wu, T.-J. Yang, and S.-J. Chang, "Terahertz multichanneled filter in a superconducting photonic crystal," *Optics Express*, Vol. 18, 27155–27166, 2010.
13. Van Duzer, T. and C. W. Turner, *Principles of Superconductive Devices and Circuits*, Edward Arnold, London, 1981.
14. Hojo, H. and A. Mase, "Dispersion relation of electromagnetic waves in one-dimensional plasma photonic crystals," *J. Plasma Fusion Res.*, Vol. 80, 89–90, 2004.
15. Hojo, H. and A. Mase, "Electromagnetic-wave transmittance characteristics in one-dimensional plasma photonic crystals," *J. Plasma Fusion Res.*, *SERIES*, Vol. 8, 477–479, 2009.
16. Li, W., Y. Zhao, R. Cui, and H. Zhang, "Plasma photonic crystal," *Font. Optoelectron. China*, Vol. 2, 103–107, 2009, and references therein.
17. Prasad, S., V. Singh, and A. K. Singh, "Dispersion characteristics and optimization of reflectivity of binary one-dimensional plasma photonic crystal having linearly graded material," *Progress In Electromagnetics Research M*, Vol. 22, 149–162, 2012.
18. Manzanares-Martinez, J., "Analytic expression for the effective plasma frequency in one-dimensional metallic-dielectric photonic crystal," *Progress In Electromagnetics Research M*, Vol. 13, 189–

202, 2010.

19. Fan, W. and L. Dong, "Tunable one-dimensional plasma photonic crystals in dielectric barrier discharge," *Phys. Plasmas*, Vol. 17, 073506, 2010.
20. Faith, J., S. P. Kuo, and J. Huang, "Frequency downshifting and trapping of an electromagnetic wave by a rapidly created spatially periodic plasma," *Phys. Rev. E*, Vol. 55, 1843–1851, 1997.
21. Kuo, S. P. and J. Faith, "Interaction of an electromagnetic wave with a rapidly created spatially periodic plasma," *Phys. Rev. E*, Vol. 56, 2143–2150, 1997.
22. Sakai, O., T. Sakaguchi, and K. Tachibana, "Verification of a plasma photonic crystal for microwaves of millimeter wavelength range using two-dimensional array of columnar microplasmas," *Appl. Phys. Lett.*, Vol. 87, 241505, 2005.
23. Sakai, O., T. Sakaguchi, and K. Tachibana, "Photonic bands in two-dimensional microplasma arrays. I. Theoretical derivation of band structure of electromagnetic waves," *J. Appl. Phys.*, Vol. 101, 073304, 2007.
24. Hung, H.-C., C.-J. Wu, T.-J. Yang, and S.-J. Chang, "Enhancement of near-infrared photonic band gap in a doped semiconductor photonic crystal," *Progress In Electromagnetics Research*, Vol. 125, 219–235, 2012.
25. Awasthi, S. K., U. Malaviya, and S. P. Ojha, "Enhancement of omnidirectional total-reflection wavelength range by using one-dimensional ternary photonic bandgap material," *J. Opt. Soc. Am. B: Optical Physics*, Vol. 23, 2566–2571, 2006.
26. Banerjee, A., "Enhanced refractometric optical sensing by using one-dimensional ternary photonic crystals," *Progress In Electromagnetics Research*, Vol. 89, 11–22, 2009.
27. Banerjee, A., "Enhanced incidence angle based spectrum tuning by using one-dimensional ternary photonic band gap structures," *Journal of Electromagnetic Waves and Applications*, Vol. 24, Nos. 8–9, 1023–1032, 2010.
28. Wu, C.-J., Y.-H. Chung, B.-J. Syu, and T.-J. Yang, "Band gap extension in a one-dimensional ternary metal-dielectric photonic crystal," *Progress In Electromagnetics Research*, Vol. 102, 81–93, 2010.
29. Dai, X. Y., Y. J. Xiang, and S. C. Wen, "Broad omnidirectional reflector in the one-dimensional ternary photonic crystals containing superconductor," *Progress In Electromagnetics Research*, Vol. 120, 17–34, 2011.

30. Prasad, S., V. Singh, and S. K. Singh, "Modal propagation characteristics of EM waves in ternary one-dimensional plasma photonic crystals," *Optik*, Vol. 121, 1520–1528, 2010.
31. Naumov, A. N. and A. M. Zheltikov, "Ternary one-dimensional photonic band gap structures: Dispersion relation, extended phase-matching abilities and attosecond outlook," *Laser Phys.*, Vol. 11, 879–884, 2001.
32. Morozov, G. V. and D. W. L. Sprung, "Floquet-Bloch waves in one-dimensional photonic crystals," *Europhysics Lett.*, Vol. 96, 54005, 2011.
33. Yeh, P., *Optical Waves in Layered Media*, Wiley, New York, 1988.
34. Morozov, G. V, F. Placido, and D. W. L. Sprung, "Absorptive photonic crystals in 1D," *J. Optics*, Vol. 13, 035102, 2011.
35. Bergmair, M., M. Huber, and K. Hingerl, "Band structure, wiener bounds and coupled surface plasmons in one dimensional photonic crystals," *Appl. Phys. Lett.*, Vol. 89, 081907–081909, 2006.
36. Naito, T., O. Saikai, and K. Tachibana, "Experimental verification of complex dispersion relation in lossy photonic crystals," *Appl. Phys. Express*, Vol. 1, 066003, 2008.